

Advancements and applications of hyperpolarized xenon MRI for chronic obstructive pulmonary disease assessment in China

Haidong Li, PhD^{#,1,2}, Hongchuang Li, PhD^{#,1,2}, Ming Zhang, PhD^{#,1,2}, Yuan Fang, PhD^{1,2}, Luyang Shen, BSc¹, Xiaoling Liu, BSc^{1,2}, Sa Xiao, PhD^{1,2}, Qingbin Zeng, PhD^{1,2}, Qian Zhou, PhD¹, Xiuchao Zhao, PhD^{1,2}, Lei Shi, MD^{1,2}, Yeqing Han, MD^{1,2}, Xin Zhou, PhD^{*,1,2,3} 

¹State Key Laboratory of Magnetic Resonance Spectroscopy and Imaging, National Center for Magnetic Resonance in Wuhan, Wuhan Institute of Physics and Mathematics, Innovation Academy for Precision Measurement Science and Technology, Chinese Academy of Sciences, Wuhan 430071, China

²University of Chinese Academy of Sciences, Beijing 100049, China

³Key Laboratory of Biomedical Engineering of Hainan Province, School of Biomedical Engineering, Hainan University, Haikou 570228, China

*Corresponding author: Xin Zhou, PhD, National Center for Magnetic Resonance in Wuhan, Wuhan Institute of Physics and Mathematics, Innovation Academy for Precision Measurement Science and Technology, Chinese Academy of Sciences, 30 West Xiaohongshan, Wuhan 430071, China (xinzhou@wipm.ac.cn)

[#]Haidong Li, Hongchuang Li, and Ming Zhang contributed equally to this work.

Abstract

Chronic obstructive pulmonary disease (COPD) is one of the leading causes of morbidity and mortality in China, highlighting the importance of early diagnosis and ongoing monitoring for effective management. In recent years, hyperpolarized ¹²⁹Xe MRI technology has gained significant clinical attention due to its ability to noninvasively and visually assess lung ventilation, microstructure, and gas-exchange function. Its recent clinical approval in China, the United States, and several European countries represents a significant advancement in pulmonary imaging. This review provides an overview of the latest developments in hyperpolarized ¹²⁹Xe MRI technology for COPD assessment in China. It covers the progress in instrument development, advanced imaging techniques, artificial intelligence-driven reconstruction methods, molecular imaging, and the application of this technology in both COPD patients and animal models. Furthermore, the review explores potential technical innovations in ¹²⁹Xe MRI and discusses future directions for its clinical applications, aiming to address existing challenges and expand the technology's impact in clinical practice.

Keywords: hyperpolarized ¹²⁹Xe MRI; COPD; pulmonary function; lung ventilation; alveolar microstructure; gas exchange; AI-driven reconstruction; molecular imaging.

Introduction

Chronic obstructive pulmonary disease (COPD) represents a critical global health challenge, marked by persistently high prevalence, substantial mortality, and significant disability burdens, with particularly severe impacts on low- and middle-income countries. According to the Global Burden of Disease Study 2021, COPD remains one of the leading causes of years lived with disability and disability-adjusted life-years worldwide, consistently ranking among the top contributors to the global disease burden from 1990 to 2021.^{1–4} In particular, China bears the heaviest COPD burden globally, with epidemiological surveys estimating over 100 million diagnosed cases and a prevalence exceeding 40% among adults aged 60 years and older.⁵ It is concerning that recent study has indicated an accelerated incidence of COPD among individuals under the age of 50 years of age due to the synergistic effects of ozone exposure and household air pollution.⁶ Consequently, it has become increasingly urgent to improved diagnostic strategies across all age groups.

Clinically, COPD is characterized by persistent respiratory symptoms and progressive airflow limitation caused by airway inflammation, remodelling, and emphysema. Its development and progression result from the interaction of multiple factors and mechanisms. It is primarily associated with the activation of inflammatory signalling pathways, immune imbalance, protease/antiprotease imbalance, and oxidative/antioxidative imbalance. During the progression of COPD, many biomarkers, such as tumour necrosis factor- α (TNF- α), interleukin-6 (IL-6), interleukin-8 (IL-8), undergo upregulation or downregulation. Conventional diagnostic approaches for COPD include pulmonary function tests (PFTs) and CT. PFTs are considered the gold standard of COPD diagnosis, but they can only provide the overall evaluation of lung function, which limits their utility in the early disease stages of COPD. CT imaging is invaluable for detecting structural pathologies like emphysema and airway remodelling; however, the associated ionizing radiation limits its routine use, particularly in younger patients.⁷

Received: 26 February 2025; Revised: 22 May 2025; Accepted: 23 May 2025

© The Author(s) 2025. Published by Oxford University Press on behalf of the British Institute of Radiology. All rights reserved. For commercial re-use, please contact reprints@oup.com for reprints and translation rights for reprints. All other permissions can be obtained through our RightsLink service via the Permissions link on the article page on our site—for further information please contact journals.permissions@oup.com.

Early diagnosis of COPD is vital for improving patient outcomes.⁸ It enables timely interventions, such as smoking cessation, personalized treatment strategies, and proactive disease management, which can slow disease progression and alleviate healthcare burdens. Yet, the insidious onset of COPD symptoms often leads to delayed diagnosis, highlighting the need for more advanced and sensitive diagnostic techniques. Over the past decades, hyperpolarized gas MRI, including ^3He , ^{83}Kr , and ^{129}Xe ,⁹⁻¹² has been proposed for pulmonary function assessment. Among these, ^{129}Xe MRI has the unique advantages for pulmonary gas-exchange assessment owing to its good solubility in blood and tissue, and its chemical shift sensitivity to its local environment.¹³⁻¹⁶ Moreover, the cost-efficient production through cryogenic air separation and long spin polarization persistence, position ^{129}Xe MRI as the preferred modality over ^3He (limited by reactor-dependent supply chains)¹⁷ and ^{83}Kr (hampered by rapid depolarization kinetics)¹⁸ for clinical applications. Hyperpolarized ^{129}Xe MRI has considerable potential for the early detection and comprehensive assessment of COPD, as it can visualize functional impairments that are not readily detected by conventional methods and has demonstrated safety and tolerability in both healthy volunteers and patients.^{19,20} Notably, the technique has been approved for clinical applications in China, United States, and some countries in Europe. A recent multinational, multicenter, and multiplatform study using ^{129}Xe MR was initiated to evaluate the longitudinal progression of COPD.²¹ It implements a standardized protocol and elaborates on implementation steps, quality control methods, and lessons learned. It also tracks a GOLD III COPD patient through 48 weeks, capturing 2 clinically significant events: an acute exacerbation (day 9) and COVID-19 infection (day 103). Quantitative ^{129}Xe MRI revealed progressive deterioration of gas-exchange function, with membrane uptake defects increasing and red blood cell (RBC) transfer deficits expanding, paralleling a decline in forced expiratory volume in one second (FEV_1).

In this review, we focus on recent advancements in hyperpolarized ^{129}Xe MRI for COPD assessment, especially in China, and discuss its potential for improving early diagnosis of the disease as well as the challenges it may face in the future.

The development of hyperpolarized ^{129}Xe MRI in China

Conventional clinical MRI relies predominantly on imaging protons within water molecules. However, the lung parenchyma, being mainly air-filled, exhibits a proton density approximately 1000 times lower than that of other tissues, resulting in very weak MR signals and challenging image acquisition.²² Hyperpolarized ^{129}Xe MRI overcomes this limitation through spin-exchange optical pumping.²³⁻²⁵ In this process, laser-polarized alkali metal electrons transfer spin polarization to ^{129}Xe nuclei via atomic collisions, generating hyperpolarized gas with a 10^4 – 10^5 -fold signal enhancement over thermal equilibrium states, enabling high-resolution visualization of pulmonary structure, ventilation, and gas-exchange dynamics.

Research on the technique of hyperpolarized ^{129}Xe MRI in China could date back to 1983, when Zeng et al²⁶ conducted pioneering theoretical investigations into the spin-exchange cross-section and efficiency between alkali metal atoms and

noble gases such as ^{129}Xe . This seminal work established the theoretical framework for subsequent technological advances. Over the ensuing decades, 2 landmark achievements were realized: the acquisition of China's first small animal ^{129}Xe lung MRI image,²⁷ followed by the successful implementation of human pulmonary ^{129}Xe MRI in 2010s with the homemade xenon gas polarizers and multi-nuclei MRI equipment.²⁸ The feasibility and safety of hyperpolarized ^{129}Xe ventilation MRI for patients with lung diseases have been investigated in China in 2010s.²⁹ During the COVID-19 pandemic, hyperpolarized ^{129}Xe MRI was first employed in China to detect impaired lung gas exchange in discharged COVID-19 patients,³⁰ and its application has since expanded globally.³¹⁻³⁵ These breakthroughs not only demonstrated the practical viability of the technology but also spurred the development of specialized equipment for translational research, fostering comprehensive studies on methodological refinements and clinical applications. Notably, clinical translation of hyperpolarized ^{129}Xe MRI has accelerated in recent years. In 2020, a ^{129}Xe gas polarizer received approval from the National Medical Products Administration in China, and in 2023, the human lung multinuclear gas MRI system (uMR780(Xe)) was also approved for clinical lung scanning in China.³⁶

Hyperpolarized ^{129}Xe MRI for COPD assessment in China

Pulmonary ventilation function assessment

Hyperpolarized ^{129}Xe MRI provides a direct and robust method for evaluating pulmonary ventilation. Upon inhalation, xenon gas diffuses into alveolar spaces, enabling precise visualization of lung ventilation, which is also the earliest and most well-established application of ^{129}Xe MRI. Unlike conventional imaging modalities, ^{129}Xe MRI is free from background interference from surrounding tissues (eg, cardiac or muscular structures), allowing unobstructed mapping of gas distribution and airflow dynamics within the lungs.^{19,37,38} This technique exhibits exceptional sensitivity in diagnosing obstructive lung diseases, such as COPD and asthma.³⁹⁻⁴¹ The ventilation function can be quantified by calculating the percentage of poorly ventilated regions in co-registered ^{129}Xe and ^1H MRI images. Quantitative metrics such as the ventilation defect percentage (VDP) are associated with the GOLD classification of COPD⁴² and have correlated strongly with PFTs.^{9,43,44} In order to characterize the heterogeneity of lung ventilation, more sophisticated methods such as the hierarchical k-means clustering algorithm⁴⁵ and linear binning³⁷ have been developed by international researchers.

In China, the technology was integrated into function-guided radiotherapy planning for lung cancer, where ventilation maps optimized radiation beam angles to spare well-ventilated lung regions, enhancing therapeutic precision while preserving respiratory function.⁴⁶

Typically, ventilation images are obtained during a subject's breath-hold, referred to as static ventilation imaging. To improve image quality, various methods have been proposed by Chinese researchers. For example, a k-space-based analysis method incorporating low-frequency boosting and high-frequency modulation to counteract magnetization loss, along with convex combination techniques in the image domain, was proposed. This approach could effectively enhance the signal-to-noise ratio (SNR) and reduce blurring in

ventilation images, particularly in patients with COPD.⁴⁷ To address challenges such as limited breath-holding capacity and suboptimal spatial resolution, a gradient echo-zigzag sequence was introduced, utilizing an accelerated zigzag k-space trajectory. This technique enabled high-resolution functional lung imaging within a clinically feasible 3.5-s acquisition window with spatial resolution of 3 mm, or 5.5-s acquisition window with spatial resolution of 2.5 mm (Figure 1), significantly improving sensitivity to impairment of ventilation function due to small airway obstructions.⁴⁸

Beyond static imaging, hyperpolarized Xe MRI has also been employed for dynamic ventilation imaging, which provides continuous structural and functional information during the respiratory cycle.⁴⁹ Dynamic imaging enhances the ability to detect early-stage obstructive lung diseases and offers a more comprehensive assessment of ventilation heterogeneity. Several dynamic ventilation imaging methods have been developed, achieving image acquisition at 202 ms per frame, which might be helpful for the early detection of obstructive lung diseases.^{50,51}

Alveolar diffusion and morphological parameters measurement

Quantitative assessment of the alveolar microstructure can be achieved by exploiting the diffusion properties of xenon gas within the alveoli. Hyperpolarized ^{129}Xe diffusion-weighted imaging (DWI) is widely employed for this purpose. By

integrating various diffusion models, such as the cylindrical model and the stretched exponential model, relevant alveolar structural parameters can be derived for pulmonary morphological evaluation.^{52,53} This approach has been successfully demonstrated in several pulmonary diseases characterized by altered alveolar structure, particularly COPD.⁵⁴⁻⁵⁶

Recent advancements in China have further expanded both the technique and applications of hyperpolarized ^{129}Xe DWI. For instance, Wang et al⁵⁷ and Ruan et al⁵⁸ applied ^{129}Xe DWI to assess elastase-induced emphysema in rat models. They reported significant differences in the apparent diffusion coefficient and other morphological parameters between emphysematous and control groups, with these parameters correlating with pulmonary histological metrics. To capture the non-Gaussian diffusion behaviour of hyperpolarized ^{129}Xe in rat lungs more effectively, a diffusion kurtosis imaging (DKI) model was introduced.⁵⁹ This DKI approach was demonstrated to be sensitive in detecting smoke-induced pulmonary lesions, including moderate emphysema and small airway diseases.

Acquisition of ^{129}Xe DWI data typically requires multiple b-values to accurately fit the diffusion model and obtain the lung's morphological parameters. In animal studies, such a long acquisition can be completed over multiple short breath-hold periods; however, in human imaging, the entire acquisition must often be completed within a single breath-hold. As a result, acceleration techniques are essential. Zhang et al⁶⁰

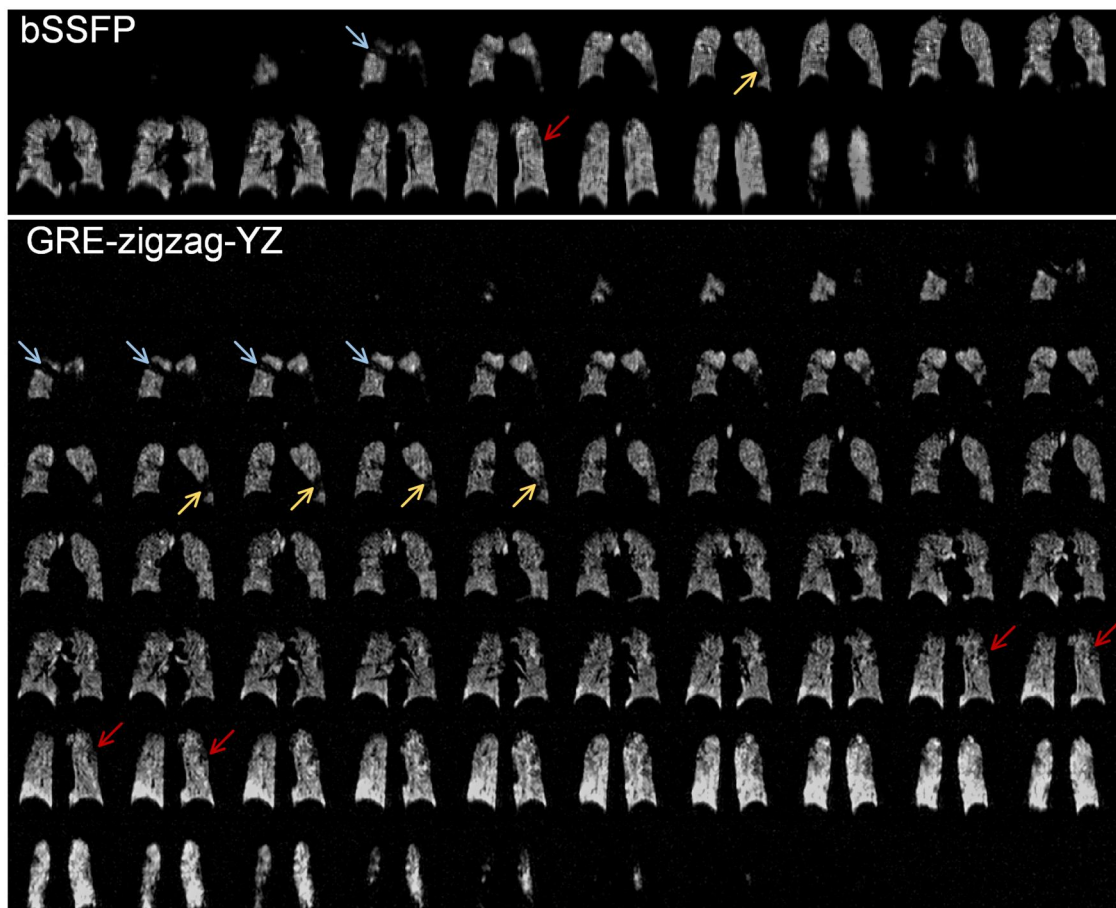


Figure 1. ^{129}Xe ventilation images obtained with balanced steady-state free precession (bSSFP) and gradient-recalled echo (GRE)-zigzag-YZ for a representative coronavirus disease 2019 patient. Blue, yellow, and red arrows indicate that more details of ventilation information are observed in the images acquired with GRE-zigzag-YZ compared with bSSFP in the corresponding slices, respectively.

applied compressed sensing (CS) to achieve a 2-fold acceleration of ^{129}Xe DWI. Based on this work, Zhou et al⁶¹ advanced the CS method by introducing a variable-sampling-ratio CS technique that attained a 4-fold acceleration. Their methods not only maintained image quality but also reduced data acquisition time significantly. Most importantly, their methods can effectively distinguish COPD patients and smokers from healthy volunteers. Recently, a technique that combines 3D golden-angle radial sampling with keyhole reconstruction has been developed to further accelerate multi-b-value ^{129}Xe DWI and achieve thinner slice imaging⁶²; the lung microstructural measurements derived from this method showed significant differences between emphysema patients and healthy subjects (see Figure 2).

Pulmonary gas-exchange function assessment

Pulmonary gas-exchange capacity can be quantitatively evaluated by measuring the diffusion efficiency of gases across the alveolar-capillary membrane. Upon inhalation, hyperpolarized ^{129}Xe exhibits 3 distinct resonance signals: in the alveolar gas phase (0 ppm), in tissue and plasma (197 ppm), and in RBCs (217 ppm).⁶³ By analysing the dynamics of xenon gas among these compartments and applying gas-exchange

models, the gas-blood exchange function of the lungs can be quantified both globally and regionally.⁶⁴⁻⁶⁶

Chemical shift saturation recovery (CSSR) was widely used for global quantifying the pulmonary gas-blood exchange function.^{16,30,67,68} In order to obtain quantitative information on gas-blood exchange, Patz,⁶⁵ Mansson,⁶⁶ and MOXE⁶⁴ models were developed internationally. This technique has been employed in China to detect subtle impairments in gas-blood exchange function caused by lung diseases, such as in radiation-induced lung injury,⁶⁹ post-COVID-19 patients,³⁰ and COPD.^{68,70} Notably, inspired by the CSSR technique, a new method was proposed for assessing pulmonary haematocrit using the properties of dissolved ^{129}Xe MR signal oscillations.⁷¹

In addition to global measurements of gas exchange using CSSR, imaging methods have also been developed in China. Li et al proposed using hyperpolarized ^{129}Xe chemical exchange saturation transfer (Hyper-CEST) to detect gas-exchange function change caused by COPD.⁷² They introduced a parameter, the pulmonary apparent gas-exchange time constant (T_{app}), and found that T_{app} showed statistically significant differences between healthy and COPD cohorts.

Additionally, an approach to concurrently image lung ventilation and gas-exchange function using hyperpolarized

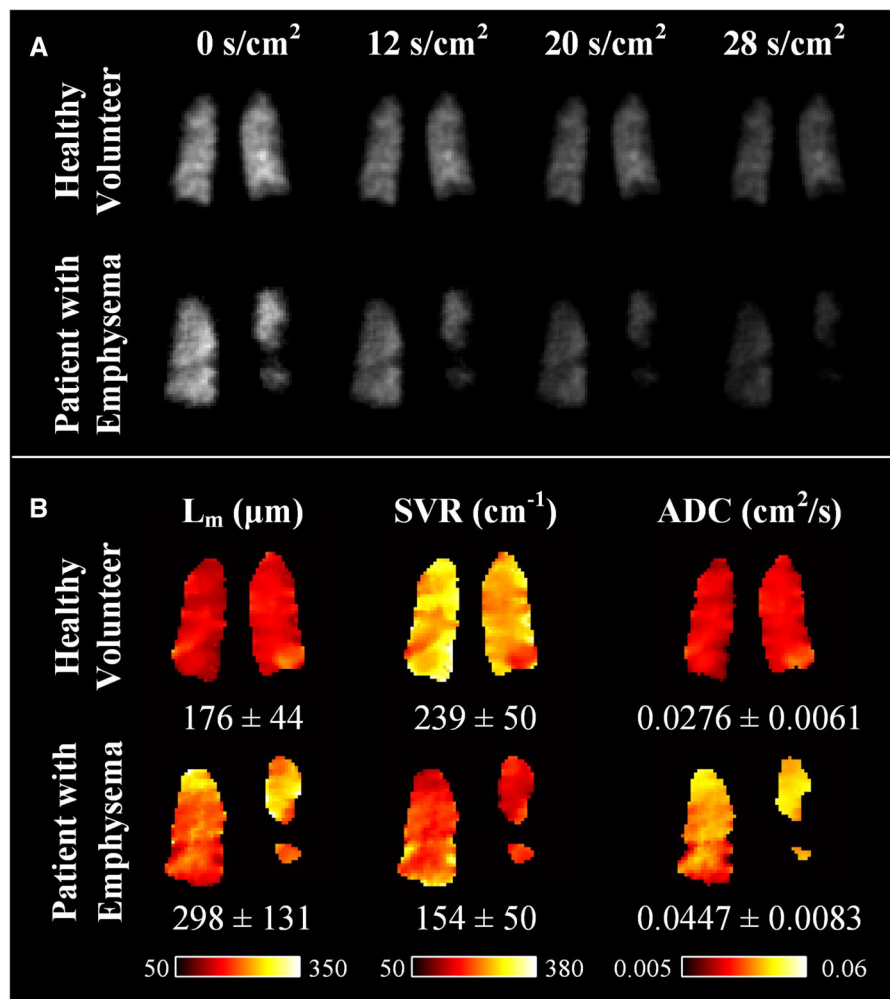


Figure 2. Representative ^{129}Xe diffusion-weighted lung images (A) and corresponding pulmonary morphological parameter maps (B) from an age-matched healthy control (AMC; 67 years old) and a patient with emphysema (70 years old), acquired via 3D golden-angle radial sampling with keyhole reconstruction diffusion-weighted imaging. Abbreviation: L_m = mean airspace chord length, ADC = apparent diffusion coefficient, SVR = alveolar surface area to volume ratio.

^{129}Xe MRI has also been developed recently.⁷³ This method involves separate excitation of ^{129}Xe signals dissolved in tissue/plasma and RBCs, simultaneous acquisition of ^{129}Xe signals in alveoli and dissolved in either tissue/plasma or RBCs, and reconstruction by modulating the phase of k-space data. The technique has been successfully verified in rats and human lungs, quantifying the septal wall thickness changes caused by lung diseases.

Comprehensive assessment of lung function in COPD with ^{129}Xe MR

A comprehensive evaluation of pulmonary function in COPD necessitates an integrated assessment of ventilation, microstructure, and gas exchange to fully understand lung physiology. Rao et al⁷⁰ utilized hyperpolarized ^{129}Xe MR to systematically assess pulmonary physiological changes induced by ageing, smoking, and COPD. Their findings indicated that structural and functional changes in the lungs due to ageing, cigarette smoking, and COPD are diverse and exhibit progressive deterioration with the accumulation of these risk factors (Figure 3). The clinical relevance of this study has been further underscored in follow-up discussions within the field.⁷⁴

In addition to smoking, a well-established risk factor for COPD, environmental exposures such as air pollution significantly contribute to the development and exacerbation of COPD. Zhang et al⁷⁵ demonstrated that hyperpolarized ^{129}Xe MRI can quantitatively assess early-stage lung damage induced by fine particulate matter ($\text{PM}_{2.5}$). Compared to the control group, although there were no significant changes in alveolar size, the exchange time constant and septal wall thickness both increased in the $\text{PM}_{2.5}$ cohort, with results consistent with quantitative histology (Figure 4). These findings demonstrated the potential of this technique for early assessment of COPD.

Benefit from the radiation-free nature, hyperpolarized ^{129}Xe MRI emerges as an ideal modality for longitudinal pulmonary monitoring in chronic respiratory diseases like COPD, given its radiation-free nature that enables safe repeated assessments. Zhang et al⁷⁶ demonstrated this clinical potential through dynamic tracking of acute lung injury (ALI) progression, revealing distinctive biomarker sensitivities: alveolar structural parameters effectively reflected dimensional changes during chronic ALI phases, while the RBC/TP ratio maintained sensitivity to gas-exchange alterations throughout the entire disease course.

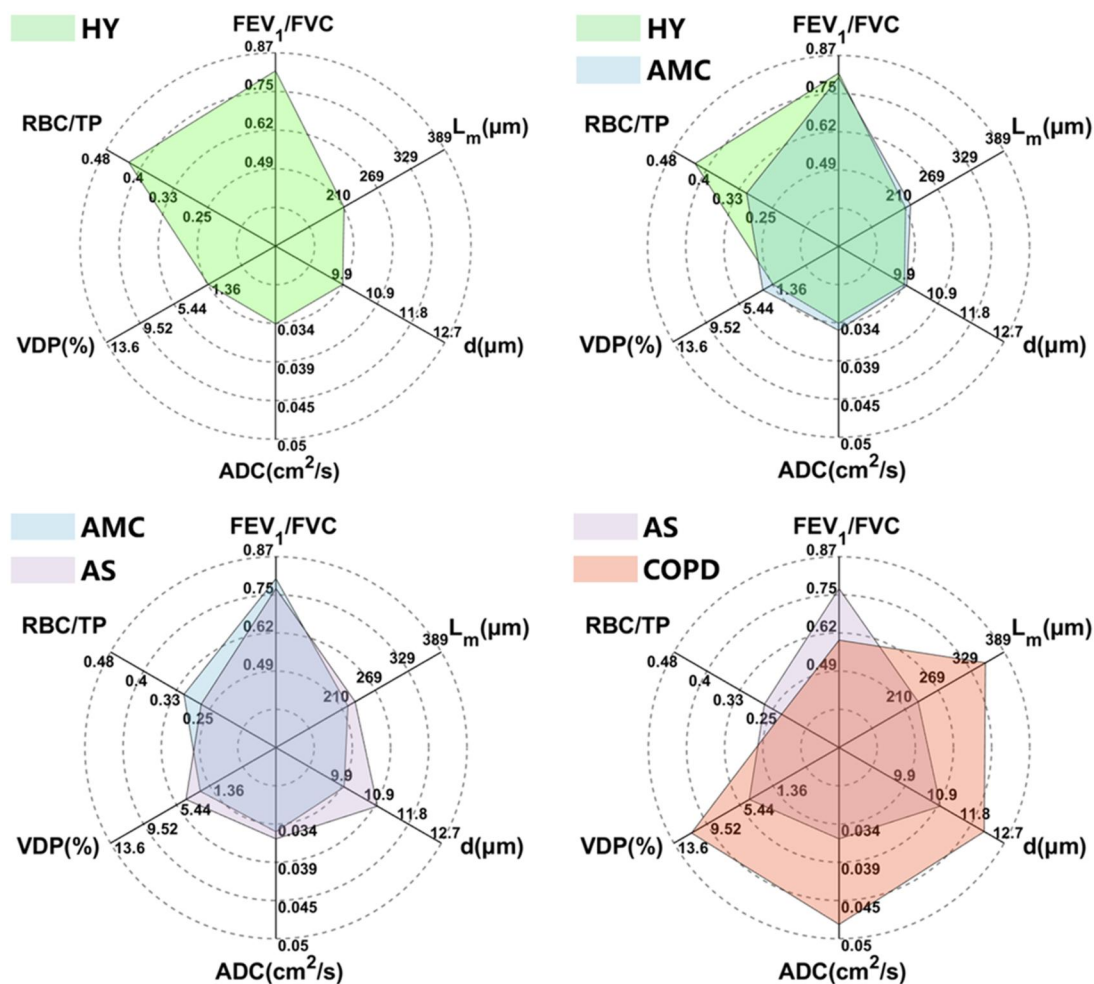


Figure 3. Radar plots used to display the primary PFTs and hyperpolarized ^{129}Xe MRI signatures associated with different groups. The mean values of the markers for each group are plotted along one of the 6 radial axes, which represent the following parameters: FEV₁/FVC ratio, ventilation defect percentage (VDP), apparent diffusion coefficient (ADC), mean airspace chord length (L_m), total septal wall thickness (d), and the ratio of xenon signal from red blood cells to tissue (RBC/TP). Abbreviations: HY = healthy young; AMC = age-matched healthy control; AS = asymptomatic smokers; COPD = chronic obstructive pulmonary disease; FEV₁/FVC = forced expiratory volume in one second / forced vital capacity.

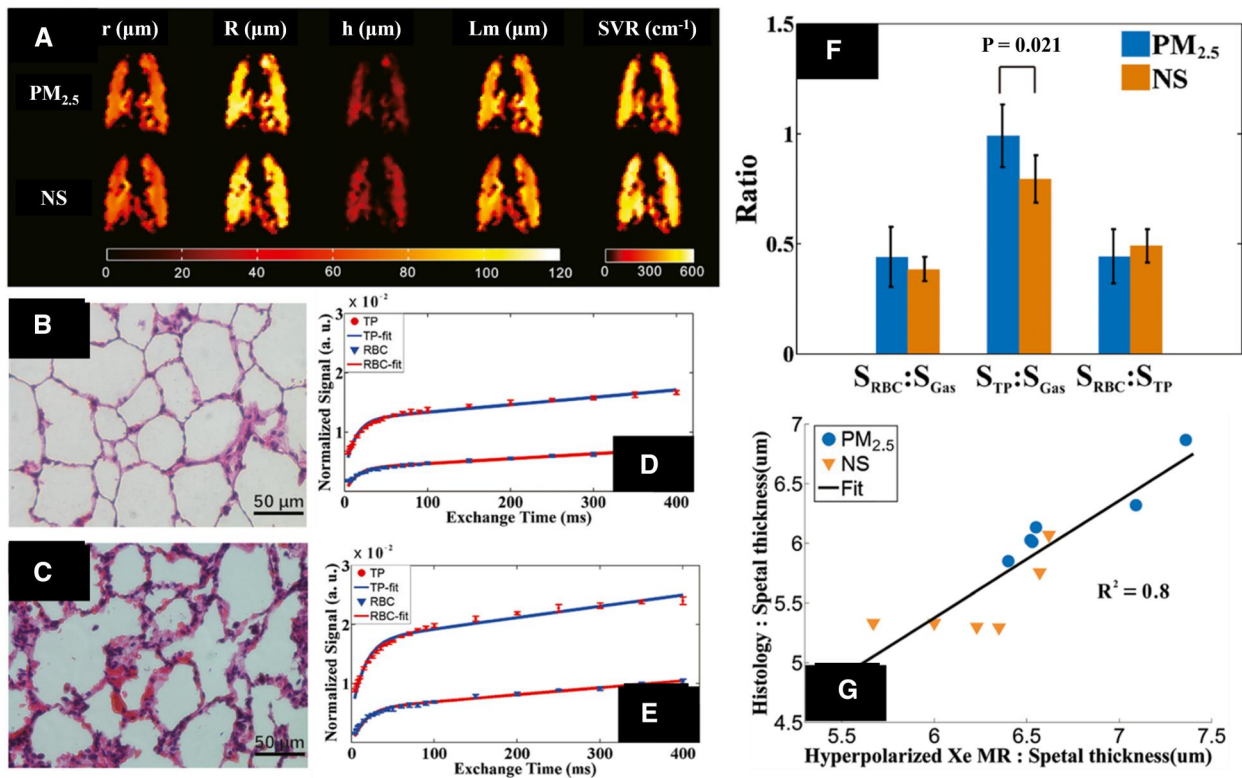


Figure 4. (A) Representative maps of the microstructure from the NS (top row) and PM_{2.5} rat groups (bottom row). H&E-stained lung tissue from representative NS (B) and PM_{2.5} rats (C). Dissolved xenon recovery curves of the representative NS rat (D) and PM_{2.5} rat (E). Comparison of RBC/gas, TP/gas, and RBC/TP between the PM_{2.5} and NS cohorts (F). Correlation of septal thickness derived by hyperpolarized ¹²⁹Xe MR and histology (G). Abbreviations: NS = normal saline; PM_{2.5} = particulate matter; SVR = alveolar surface area to volume ratio; RBC/TP = the ratio of xenon signal from red blood cells to tissue; TP = tissue/plasma.

Artificial intelligence-driven innovations in COPD diagnosis with hyperpolarized ¹²⁹Xe MRI

While hyperpolarized gas MRI offers unparalleled insights into pulmonary structure and function for COPD evaluation, its clinical translation has been hindered by prolonged acquisition times (10–20 s per scan) and noise-related artefacts. Cutting-edge artificial intelligence (AI) methodologies are now addressing these limitations through 3 synergistic pathways: accelerated reconstruction, noise-robust enhancement, and quantitative functional analysis.⁷⁷

Duan et al's⁷⁸ cascaded convolutional neural networks CNNs model achieved fast and accurate reconstruction of human lung ventilation MRI from highly undersampled k-space (4×). Subsequent refinement via a cascaded deep cascade residual dense network (DC-RDN) model achieved 4× acceleration in gas multiple *b*-value diffusion-weighted MRI for lung morphometry.⁷⁹ The DC-RDN is able to provide both high-quality reconstructed images and good preservation of quantitative microstructural information in both healthy volunteers and patients with COPD (Figure 5). To further accelerate the ¹²⁹Xe MRI, Li et al⁸⁰ proposed an encoding-enhanced complex CNN (EN²-CNN) that leverages the encoding properties of k-space data to improve reconstruction performance. By utilizing the inherent characteristics of k-space data, EN²-CNN achieves higher quality image reconstruction, which is crucial for accurate diagnosis and assessment of COPD. These advancements in MRI reconstruction techniques have significantly accelerated hyperpolarized ¹²⁹Xe MRI, making the diagnosis of COPD faster and more efficient.

Beyond acceleration, AI-driven noise suppression and functional quantification are revolutionizing hyperpolarized MRI's diagnostic precision. Shi et al⁸¹ proposed a hybrid transformer-CNN network (HTC-net) for MRI denoising targeting Rician noise. By combining the strengths of transformer and CNN, HTC-net effectively captures long-range information and maintains local details, resulting in higher quality images. This method enhances the SNR and improves the clarity of the images, providing more accurate and reliable data for clinical decision-making. Furthermore, Li et al⁸² proposed a complementation-reinforced network (RSNet) that integrates reconstruction and segmentation tasks to improve the precision of VDP. By sharing encoder weights and utilizing a feature-selecting block, RSNet demonstrates superior performance in identifying ventilated defects, which is crucial for COPD diagnosis. This method not only enhances image quality but also improves the accuracy of quantitative assessments, providing more reliable data for clinical decision-making.

The potential of ¹²⁹Xe molecular imaging for early detection of COPD

While hyperpolarized ¹²⁹Xe MRI is a powerful tool for detecting respiratory system diseases, ¹²⁹Xe is an inert gas and does not inherently enable specific detection or molecular-level imaging. Molecular cages that can trap xenon atoms, such as cryptophane-A,^{83–85} cucurbit[6]uril,⁸⁶ metal-organic frameworks,^{87–89} metal-organic layers,⁹⁰ could generate a characteristic peak distinct from dissolved xenon or xenon gas (Figure 6). This provides a promising avenue for

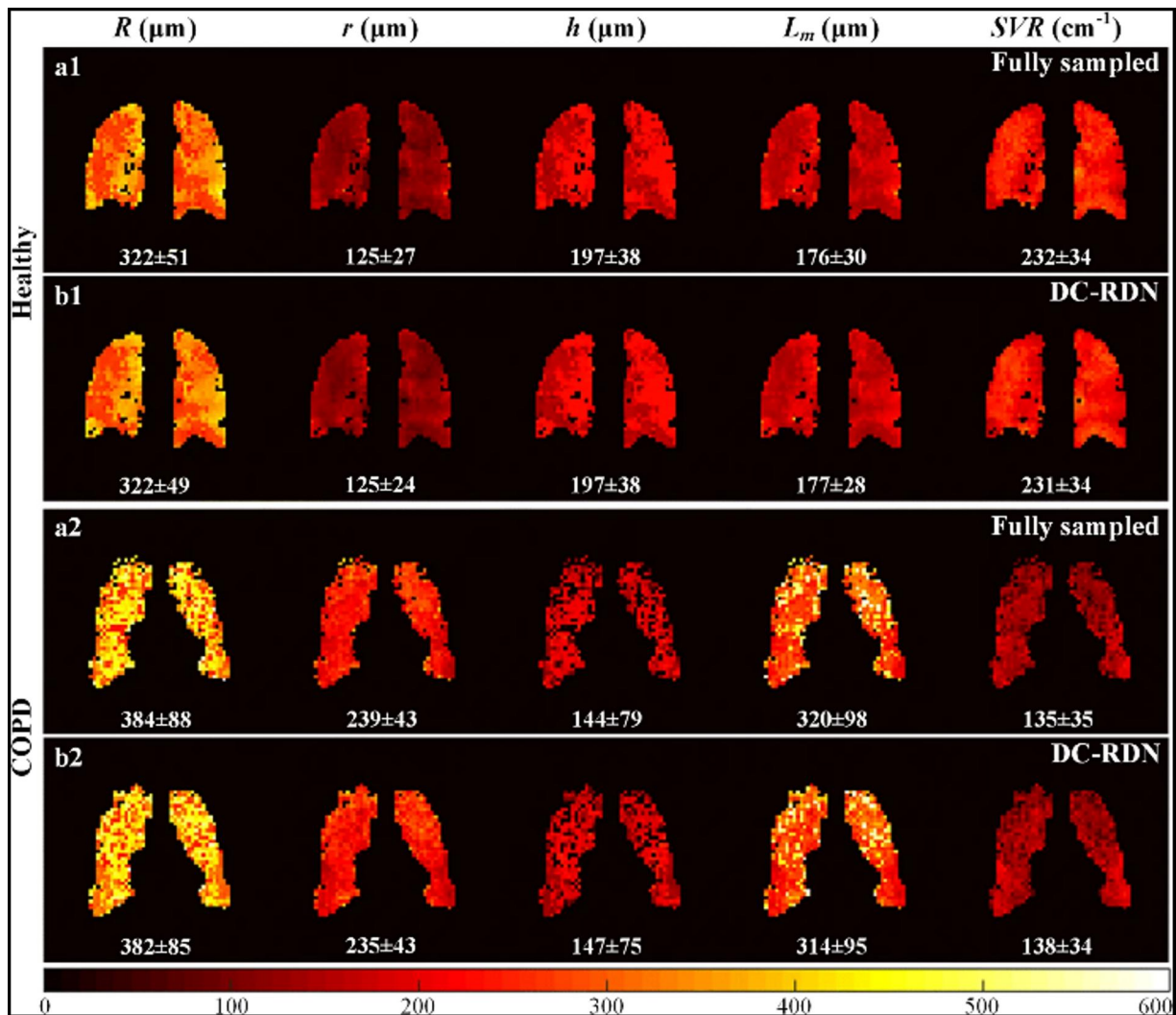


Figure 5. Lung morphometry maps derived from the fully sampled and DC-RDN reconstructed images. Abbreviations: COPD = chronic obstructive pulmonary disease; DC-RDN = deep cascade of residual dense network; SVR = alveolar surface area to volume ratio.

hyperpolarized ^{129}Xe MRI as a potential molecular imaging modality.

In recent years, researchers in China have developed a series of hyperpolarized ^{129}Xe molecular probes for detecting and imaging biomolecules in biological systems.^{91–96} These probes exhibit high selectivity and sensitivity with the best performance demonstrating an exceptional detection threshold as low as 100 picomolar (pM), offering great potential for trace biomolecule detection in biological systems. Combining the detection and analysis of multiple biological markers may provide more significant insights than relying on a single marker alone. Although the field of molecular probe imaging is still in its infancy, in the future, hyperpolarized ^{129}Xe molecular probes are expected to be used for detecting and imaging COPD—related biomarkers, monitoring COPD activity and progression, and guiding treatment. This could provide a novel way to diagnose COPD, making it a promising area for further research.

Future prospects and conclusions

Hyperpolarized ^{129}Xe MRI represents a groundbreaking advancement in the evaluation of COPD, offering high-

resolution visualization of lung physiology to comprehensively assess ventilation patterns, structural morphology, and gas-exchange efficiency. Unlike conventional imaging modalities, this technique eliminates exposure to ionizing radiation, rendering it uniquely suited for longitudinal monitoring of disease progression, therapeutic response, and early intervention strategies.⁹⁷

To translate its potential into routine clinical practice, the establishment of standardized protocols for patient preparation, image acquisition, and data analysis is imperative to ensure reproducibility and cross-study comparability.⁹⁸ Integration of rapid imaging sequences, such as CS or parallel imaging, could further enhance scan efficiency while preserving diagnostic resolution. Concurrently, multicenter clinical trials are warranted to establish normative reference values, validate diagnostic thresholds, and identify imaging biomarkers for personalized therapeutic strategies. Technological innovations, including optimized radiofrequency coils, next-generation polarizers, and advanced reconstruction algorithms, will improve SNR and imaging sensitivity. Additionally, the development of a standardized lung atlas, analogous to neuroimaging templates, would enable automated quantification of regional ventilation defects

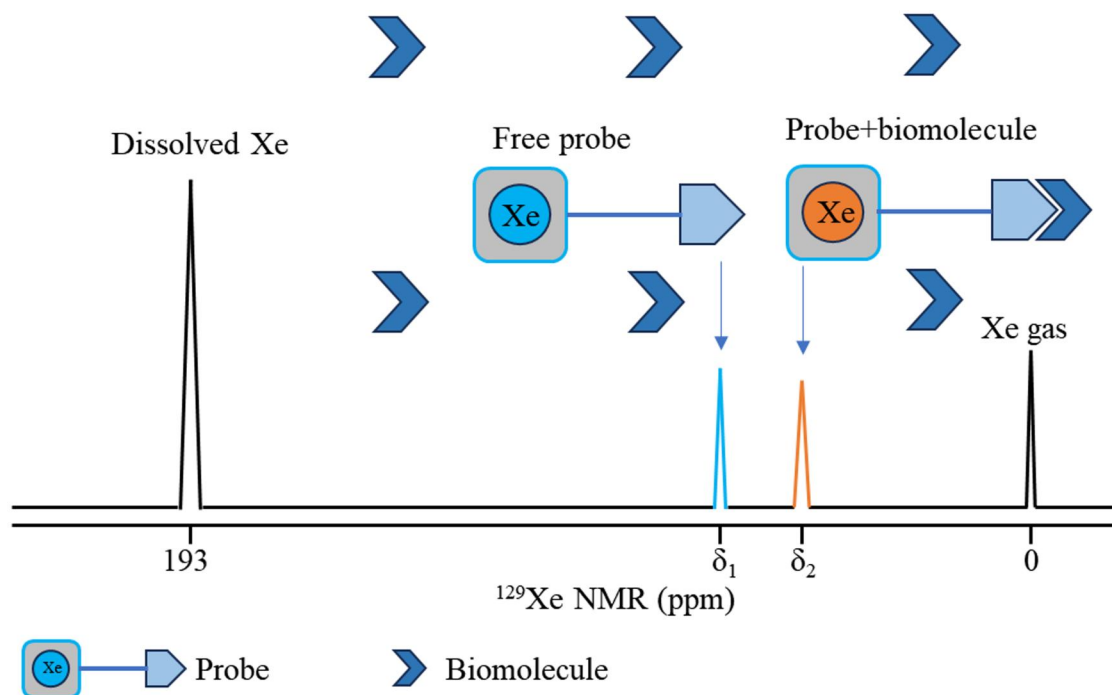


Figure 6. Schematic diagram of hyperpolarized ^{129}Xe probe for biomolecules detection. The peak at 193 ppm corresponding to dissolved ^{129}Xe in water, and peak at 0 ppm corresponding to the ^{129}Xe gas, the peak at δ_1 corresponding to the entrapped ^{129}Xe in free probe. After the probe bind to biomolecules, a new peak generated at δ_2 . All chemical shifts are referenced to that of xenon gas.

and gas-transfer abnormalities, enhancing diagnostic precision and inter-institutional consistency.

The integration of ^{129}Xe MRI with complementary modalities, such as CT, PET, and molecular imaging, may provide a multiparametric assessment of pulmonary structure, function, and molecular activity, thereby improving diagnostic accuracy and mechanistic insights. These advancements align with China's national health priorities, particularly the Healthy China 2030 initiative, which emphasizes reducing mortality from chronic respiratory diseases and enhancing patient quality of life.⁹⁹ The noninvasive, repeatable nature of hyperpolarized ^{129}Xe MRI positions it as a strategic tool for achieving these objectives through early disease detection, precise monitoring, and tailored therapeutic regimens.

While challenges persist in protocol harmonization, infrastructure development, and cost-effectiveness, hyperpolarized ^{129}Xe MRI holds transformative potential for COPD management. Several academic centres and hospitals have jointly drafted a multicenter ^{129}Xe MRI clinical trials consortium for multisite trials, aiming to promote standardization and harmonization of this technique in clinical practice. In China, to address these challenges, radiologists and researchers have collaboratively developed a consensus statement on the standardized clinical application of hyperpolarized ^{129}Xe pulmonary functional MRI.¹⁰⁰ This document provides detailed professional recommendations regarding hardware selection, personnel requirements, imaging sequences and parameters, and data processing methods for clinical ^{129}Xe MRI. Besides the consensus, AI-driven automation and targeted training programmes can also mitigate expertise gaps in the future. To ensure equitable access to this advanced imaging modality, strategies such as platform sharing and cost-reduction initiatives are essential. These measures can facilitate adoption across varied socioeconomic groups, supporting a more equitable distribution of respiratory healthcare resources.

Funding

This work is supported by National Natural Science Foundation of China (82127802, 82372150, 82441015, 82202119), the Strategic Priority Research Program of the Chinese Academy of Sciences (XDC0170000, XDB0540000), Key Research Program of Frontier Sciences, CAS (ZDBS-LY-JSC004), Hubei Provincial Key Technology Foundation of China (2021ACA013), Major Program (JD) of Hubei Province (2023BAA021) and Hubei Provincial Outstanding Youth Fund (2023AFA112, 2022CFA050). Haidong Li and Xiuchao Zhao acknowledge the support from Youth Innovation Promotion Association, CAS (2020330 and 2021330).

Conflicts of interest

The authors have no conflicts to disclose.

References

1. Vos T, Allen C, Arora M, et al. Global, regional, and national incidence, prevalence, and years lived with disability for 310 diseases and injuries, 1990–2015: a systematic analysis for the global burden of disease study 2015. *Lancet*. 2016; 388:1545-1602.
2. Wang H, Naghavi M, Allen C, et al. Global, regional, and national life expectancy, all-cause mortality, and cause-specific mortality for 249 causes of death, 1980–2015: a systematic analysis for the global burden of disease study 2015. *Lancet*. 2016;388:1459-1544.
3. Global incidence, prevalence, years lived with disability (YLDs), disability-adjusted life-years (DALYs), and healthy life expectancy (HALE) for 371 diseases and injuries in 204 countries and territories and 811 subnational locations, 1990-2021: a systematic analysis for the Global Burden of Disease Study 2021.

- Lancet*. 2024;403:2133-2161. [https://doi.org/10.1016/s0140-6736\(24\)00757-8](https://doi.org/10.1016/s0140-6736(24)00757-8)
4. Xu J, Ji Z, Zhang P, Chen T, Xie Y, Li J. Disease burden of COPD in the Chinese population: a systematic review. *Thorax*. 2023;17:17534666231218899. <https://doi.org/10.1177/17534666231218899>
 5. Wang C, Xu J, Yang L, et al. Prevalence and risk factors of chronic obstructive pulmonary disease in China (the China Pulmonary Health [CPH] study): a national cross-sectional study. *Lancet*. 2018;391:1706-1717.
 6. Xing Z, Yang T, Shi S, et al. Combined effect of ozone and household air pollution on COPD in people aged less than 50 years old. *Thorax*. 2023;79:35-42. <https://doi.org/10.1136/thorax-2022-219691>
 7. Raoof S, Shah M, Make B, et al. Lung imaging in COPD part 1: clinical usefulness. *Chest*. 2023;164:69-84. <https://doi.org/10.1016/j.chest.2023.03.007>
 8. Lin CH, Cheng SL, Chen CZ, Chen CH, Lin SH, Wang HC. Current progress of COPD early detection: key points and novel strategies. *Int J Chron Obstruct Pulmon Dis*. 2023;18:1511-1524. <https://doi.org/10.2147/copd.S413969>
 9. Stewart NJ, Chan HF, Hughes PJC, et al. Comparison of ^3He and ^{129}Xe MRI for evaluation of lung microstructure and ventilation at 1.5T. *J Magn Reson Imaging*. 2018;48:632-642. <https://doi.org/10.1002/jmri.25992>
 10. Lilburn DM, Lesbats C, Six JS, et al. Hyperpolarized ^{83}Kr magnetic resonance imaging of alveolar degradation in a rat model of emphysema. *J R Soc Interface*. 2015;12. <https://doi.org/10.1098/rsif.2015.0192>
 11. Hughes-Riley T, Six JS, Lilburn DML, et al. Cryogenics free production of hyperpolarized ^{129}Xe and ^{83}Kr for biomedical MRI applications. *J Magn Reson*. 2013;237:23-33. <https://doi.org/10.1016/j.jmr.2013.09.008>
 12. Cleveland ZI, Pavlovskaya GE, Elkins ND, Stupic KF, Repine JE, Meersmann T. Hyperpolarized ^{83}Kr MRI of lungs. *J Magn Reson*. 2008;195:232-7. <https://doi.org/10.1016/j.jmr.2008.09.020>
 13. Qing K, Ruppert K, Jiang Y, et al. Regional mapping of gas uptake by blood and tissue in the human lung using hyperpolarized xenon-129 MRI. *J Magn Reson Imaging*. 2014;39:346-59. <https://doi.org/10.1002/jmri.24181>
 14. Collier GJ, Eaden JA, Hughes PJC, et al. Dissolved ^{129}Xe lung MRI with four-echo 3D radial spectroscopic imaging: quantification of regional gas transfer in idiopathic pulmonary fibrosis. *Magn Reson Med*. 2021;85:2622-2633. <https://doi.org/10.1002/mrm.28609>
 15. Kammerman J, Hahn AD, Cadman RV, Malkus A, Mummy D, Fain SB. Transverse relaxation rates of pulmonary dissolved-phase hyperpolarized Xe as a biomarker of lung injury in idiopathic pulmonary fibrosis. *Magn Reson Med*. 2020;84:1857-1867. <https://doi.org/10.1002/mrm.28246>
 16. Zanette B, Santyr G. Accelerated interleaved spiral-IDEAL imaging of hyperpolarized ^{129}Xe for parametric gas exchange mapping in humans. *Magn Reson Med*. 2019;82:1113-1119. <https://doi.org/10.1002/mrm.27765>
 17. Kaushik SS, Freeman MS, Cleveland ZI, et al. Probing the regional distribution of pulmonary gas exchange through single-breath gas- and dissolved-phase ^{129}Xe MR imaging. *J Appl Physiol*. 2013;115:850-60. <https://doi.org/10.1152/jappphysiol.00092.2013>
 18. Rogers NJ, Hill-Casey F, Stupic KF, et al. Molecular hydrogen and catalytic combustion in the production of hyperpolarized ^{83}Kr and ^{129}Xe MRI contrast agents. *Proc Natl Acad Sci U S A*. 2016;113:3164-8. <https://doi.org/10.1073/pnas.1600379113>
 19. Walkup LL, Thomen RP, Akinyi TG, et al. Feasibility, tolerability and safety of pediatric hyperpolarized ^{129}Xe magnetic resonance imaging in healthy volunteers and children with cystic fibrosis. *Pediatr Radiol*. 2016;46:1651-1662. <https://doi.org/10.1007/s00247-016-3672-1>
 20. Driehuys B, Martinez-Jimenez S, Cleveland ZI, et al. Chronic obstructive pulmonary disease: safety and tolerability of hyperpolarized ^{129}Xe MR imaging in healthy volunteers and patients. *Radiology*. 2012;262:279-89. <https://doi.org/10.1148/radiol.11102172>
 21. Driehuys B, Zhang S, Bechtel A, et al. Design and implementation of a multi-center trial of ^{129}Xe gas exchange MRI and MRS to evaluate longitudinal progression of COPD. *J Magn Reson Imaging*. 2025. <https://doi.org/10.1002/jmri.29769>
 22. Yang Y, Yue S, Shen L, et al. Ultrasensitive ^{129}Xe magnetic resonance imaging: from clinical monitoring to molecular sensing. *Adv Sci (Weinh)*. 2025:e2413426. <https://doi.org/10.1002/advs.202413426>
 23. Zhou X, Luo J, Sun X, et al. Experiment and dynamic simulations of radiation damping of laser-polarized liquid ^{129}Xe at low magnetic field in a flow system. *Appl Magn Reson*. 2004;26:327-337.
 24. Zhou X, Luo J, Sun X-p, et al. Enhancement of solid-state proton NMR via the spin-polarization-induced nuclear Overhauser effect with laser-polarized xenon. *Phys Rev B*. 2004;70. <https://doi.org/10.1103/PhysRevB.70.052405>
 25. Zhou X, Sun XP, Luo J, Zeng XZ, Liu ML, Zhan MS. Production of hyperpolarized ^{129}Xe gas without nitrogen by optical pumping at ^{133}Cs D2 line in flow system. *Chin Phys Lett*. 2004;21:1501-1503.
 26. Zeng X, Wu Z, Call T, Miron E, Schreiber D, Happer W. Experimental determination of the rate constants for spin exchange between optically pumped K, Rb, and Cs atoms and ^{129}Xe nuclei in alkali-metal-noble-gas van der Waals molecules. *Phys Rev A*. 1985;31:260-278. <https://doi.org/10.1103/physreva.31.260>
 27. reporter XNA. Chinese Academy of Sciences magnetic resonance imaging machine 'lights up the lungs'. *Science and Technology Daily*. August 2, 2013. https://digitalpaper.stdaily.com/http_www.kjrb.com/kjrb/html/2013-08/02/content_216400.htm?div=-1
 28. Ding J, Lu W. The Chinese Academy of Sciences has developed a magnetic resonance imaging system for early detection of lung disease. *Chinese Science News*. September 8. <https://news.science.net.cn/sbhtmlnews/2015/9/304088.shtml>
 29. Yang H, Wang K, Zhang H, Xie J, Wu G, Zhou X. Human pulmonary hyperpolarized ^{129}Xe MRI: a preliminary study. *Chin Phys Lett*. 2018;35. <https://doi.org/10.1088/0256-307x/35/5/058701>
 30. Li H, Zhao X, Wang Y, et al. Damaged lung gas exchange function of discharged COVID-19 patients detected by hyperpolarized ^{129}Xe MRI. *Sci Adv*. 2021;7:eabc8180. <https://doi.org/10.1126/sciadv.abc8180>
 31. Grist JT, Chen M, Collier GJ, et al. Hyperpolarized ^{129}Xe MRI abnormalities in dyspneic patients 3 months after COVID-19 pneumonia: preliminary results. *Radiology*. 2021;301:E353-E360. <https://doi.org/10.1148/radiol.2021210033>
 32. Grist JT, Collier GJ, Walters H, et al. Lung abnormalities detected with hyperpolarized ^{129}Xe MRI in patients with long COVID. *Radiology*. 2022;305:709-717. <https://doi.org/10.1148/radiol.220069>
 33. Matheson AM, McIntosh MJ, Kooner HK, et al. Persistent ^{129}Xe MRI pulmonary and CT vascular abnormalities in symptomatic individuals with post-acute COVID-19 syndrome. *Radiology*. 2022;305:466-476. <https://doi.org/10.1148/radiol.220492>
 34. Matheson AM, McIntosh MJ, Kooner HK, et al. Longitudinal follow-up of postacute COVID-19 syndrome: DLCO, quality-of-life and MRI pulmonary gas-exchange abnormalities. *Thorax*. 2023;78:418-421. <https://doi.org/10.1136/thorax-2022-219378>
 35. Kooner HK, McIntosh MJ, Matheson AM, et al. Postacute COVID-19 syndrome: (129)Xe MRI ventilation defects and respiratory outcomes 1 year later. *Radiology*. 2023;307:e222557. <https://doi.org/10.1148/radiol.222557>

36. The world's first lung gas magnetic resonance imaging system has been approved for market. *Wuhan Branch of Chinese Academy of Sciences*. September 26, 2023. Accessed January 18, 2025. http://www.whb.cas.cn/xw/kyjz/202310/t20231012_6899702.html
37. He M, Driehuis B, Que LG, Huang Y-CT. Using hyperpolarized ^{129}Xe MRI to quantify the pulmonary ventilation distribution. *Acad Radiol*. 2016;23:1521-1531. <https://doi.org/10.1016/j.acra.2016.07.014>
38. Thomen RP, Walkup LL, Roach DJ, Cleveland ZI, Clancy JP, Woods JC. Hyperpolarized Xe-129 for investigation of mild cystic fibrosis lung disease in pediatric patients. *J Cyst Fibros*. 2017;16:275-282. <https://doi.org/10.1016/j.jcf.2016.07.008>
39. Virgincar RS, Cleveland ZI, Sivaram Kaushik S, et al. Quantitative analysis of hyperpolarized ^{129}Xe ventilation imaging in healthy volunteers and subjects with chronic obstructive pulmonary disease. *NMR Biomed*. 2013;26:424-435. <https://doi.org/10.1002/nbm.2880>
40. Tanabe N, Nakagawa H, Sakao S, et al. Lung imaging in COPD and asthma. *Respir Investig*. 2024;62:995-1005. <https://doi.org/10.1016/j.resinv.2024.08.014>
41. Pilgrim-Morris JH, Smith LJ, Marshall H, et al. A framework for modelling whole-lung and regional transfer factor of the lung for carbon monoxide using hyperpolarised xenon-129 lung magnetic resonance imaging. *ERJ Open Res*. 2025;11. <https://doi.org/10.1183/23120541.00442-2024>
42. Davis C, Sheikh K, Pike D, et al. Ventilation heterogeneity in never-smokers and COPD: comparison of pulmonary functional magnetic resonance imaging with the poorly communicating fraction derived from plethysmography. *Acad Radiol*. 2016;23:398-405. <https://doi.org/10.1016/j.acra.2015.10.022>
43. McIntosh MJ, Biancaniello A, Kooner HK, et al. ^{129}Xe MRI ventilation defects in asthma: what is the upper limit of normal and minimal clinically important difference? *Acad Radiol*. 2023;30:3114-3123. <https://doi.org/10.1016/j.acra.2023.03.010>
44. Lin N, Roach DJ, Willmerring MM, et al. ^{129}Xe MRI as a measure of clinical disease severity for pediatric asthma. *J Allergy Clin Immunol*. 2021;147:2146-2153. <https://doi.org/10.1016/j.jaci.2020.11.010>
45. Kirby M, Heydarian M, Svenningsen S, et al. Hyperpolarized ^3He magnetic resonance functional imaging semiautomated segmentation. *Acad Radiol*. 2012;19:141-52. <https://doi.org/10.1016/j.acra.2011.10.007>
46. Ding Y, Yang L, Zhou Q, et al. A pilot study of function-based radiation therapy planning for lung cancer using hyperpolarized xenon-129 ventilation MRI. *J Appl Clin Med Phys*. 2022;23:e13502. <https://doi.org/10.1002/acm2.13502>
47. Deng H, Duan C, Xiao S, et al. k-space-based enhancement of pulmonary hyperpolarized ^{129}Xe ventilation images. *IEEE Trans Instrum Meas*. 2019;68:3950-3961. <https://doi.org/10.1109/TIM.2018.2886097>
48. Fang Y, Li H, Shen L, et al. Rapid pulmonary ^{129}Xe ventilation MRI of discharged COVID-19 patients with zigzag sampling. *Magn Reson Med*. 2024;92:956-966. <https://doi.org/10.1002/mrm.30120>
49. Li H, Li H, Fan L, et al. Dynamic ventilation functional MRI of the lung with sub-millimeter spatial resolution and millisecond temporal resolution. *Sci Bull*. 2025;<https://doi.org/10.1016/j.scib.2025.05.014>
50. Xiao S, Deng H, Duan C, et al. Considering low-rank, sparse and gas-inflow effects constraints for accelerated pulmonary dynamic hyperpolarized ^{129}Xe MRI. *J Magn Reson*. 2018;290:29-37. <https://doi.org/10.1016/j.jmr.2018.03.003>
51. Xiao S, Deng H, Duan C, et al. Highly and adaptively undersampling pattern for pulmonary hyperpolarized ^{129}Xe dynamic MRI. *IEEE Trans Med Imaging*. 2019;38:1240-1250. <https://doi.org/10.1109/TMI.2018.2882209>
52. Sukstanskii AL, Yablonskiy DA. Lung morphometry with hyperpolarized ^{129}Xe : theoretical background. *Magn Reson Med*. 2012;67:856-66. <https://doi.org/10.1002/mrm.23056>
53. Chan HF, Stewart NJ, Parra-Robles J, Collier GJ, Wild JM. Whole lung morphometry with 3D multiple b-value hyperpolarized gas MRI and compressed sensing. *Magn Reson Med*. 2017;77:1916-1925. <https://doi.org/10.1002/mrm.26279>
54. Ouriadov A, Farag A, Kirby M, McCormack DG, Parraga G, Santyr GE. Lung morphometry using hyperpolarized ^{129}Xe apparent diffusion coefficient anisotropy in chronic obstructive pulmonary disease. *Magn Reson Med*. 2013;70:1699-706. <https://doi.org/10.1002/mrm.24595>
55. Ouriadov A, Guo F, McCormack DG, Parraga G. Accelerated ^{129}Xe MRI morphometry of terminal airspace enlargement: Feasibility in volunteers and those with alpha-1 antitrypsin deficiency. *Magn Reson Med*. 2020;84:416-426. <https://doi.org/10.1002/mrm.28091>
56. Mammarrappallil JG, Rankine L, Wild JM, Driehuis B. New developments in imaging Idiopathic Pulmonary Fibrosis with hyperpolarized Xenon MRI. *J Thorac Imaging*. 2019;34:136-150. <https://doi.org/10.1097/rti.0000000000000392>
57. Wang K, Pan T, Yang H, et al. Assessment of pulmonary microstructural changes by hyperpolarized ^{129}Xe diffusion-weighted imaging in an elastase-instilled rat model of emphysema. *J Thorac Dis*. 2017;9:2572-2578. <https://doi.org/10.21037/jtd.2017.08.39>
58. Ruan W, Zhong J, Wang K, et al. Detection of the mild emphysema by quantification of lung respiratory airways with hyperpolarized xenon diffusion MRI. *J Magn Reson Imaging*. 2017;45:879-888. <https://doi.org/10.1002/jmri.25408>
59. Ruan W, Zhong J, Guan Y, et al. Detection of smoke-induced pulmonary lesions by hyperpolarized ^{129}Xe diffusion kurtosis imaging in rat models. *Magn Reson Med*. 2017;78:1891-1899. <https://doi.org/10.1002/mrm.26566>
60. Zhang H, Xie J, Xiao S, et al. Lung morphometry using hyperpolarized ^{129}Xe multi-b diffusion MRI with compressed sensing in healthy subjects and patients with COPD. *Med Phys*. 2018;45:3097-3108. <https://doi.org/10.1002/mp.12944>
61. Zhou Q, Li H, Rao Q, et al. Assessment of pulmonary morphometry using hyperpolarized ^{129}Xe diffusion-weighted MRI with variable-sampling-ratio compressed sensing patterns. *Med Phys*. 2023;50:867-878. <https://doi.org/10.1002/mp.16018>
62. Shen L, Li H, Fang Y. Hyperpolarized ^{129}Xe diffusion-weighted MRI of the lung with 3D golden-angle radial sampling and keyhole reconstruction. *Med Phys*. 2025. <https://doi.org/10.1002/mp.17719>
63. Kaushik SS, Robertson SH, Freeman MS, et al. Single-breath clinical imaging of hyperpolarized ^{129}Xe in the airspaces, barrier, and red blood cells using an interleaved 3D radial 1-point Dixon acquisition. *Magn Reson Med*. 2016;75:1434-43. <https://doi.org/10.1002/mrm.25675>
64. Chang YV. MOXE: a model of gas exchange for hyperpolarized ^{129}Xe magnetic resonance of the lung. *Magn Reson Med*. 2013;69:884-90. <https://doi.org/10.1002/mrm.24304>
65. Patz S, Muradyan I, Hrovat MI, et al. Diffusion of hyperpolarized ^{129}Xe in the lung: a simplified model of ^{129}Xe septal uptake and experimental results. *New J Phys*. 2011;13. <https://doi.org/10.1088/1367-2630/13/1/015009>
66. Mansson S, Wolber J, Driehuis B, Wollmer P, Golman K. Characterization of diffusing capacity and perfusion of the rat lung in a lipopolysaccharide disease model using hyperpolarized ^{129}Xe . *Magn Reson Med*. 2003;50:1170-9. <https://doi.org/10.1002/mrm.10649>
67. Ruppert K, Brookeman JR, Hagspiel KD, Driehuis B, Mugler JP, 3rd. NMR of hyperpolarized ^{129}Xe in the canine chest: spectral dynamics during a breath-hold. *NMR Biomed*. 2000;13:220-8. [https://doi.org/10.1002/1099-1492\(200006\)13:4<220::aid-nbm638>3.0.co;2-f](https://doi.org/10.1002/1099-1492(200006)13:4<220::aid-nbm638>3.0.co;2-f)
68. Xie J, Li H, Zhang H, et al. Single breath-hold measurement of pulmonary gas exchange and diffusion in humans with hyperpolarized ^{129}Xe MR. *NMR Biomed*. 2019;32:e4068. <https://doi.org/10.1002/nbm.4068>

69. Li H, Zhang Z, Zhao X, Sun X, Ye C, Zhou X. Quantitative evaluation of radiation-induced lung injury with hyperpolarized xenon magnetic resonance. *Magn Reson Med.* 2016;76:408-16. <https://doi.org/10.1002/mrm.25894>
70. Rao QC, Li HD, Zhou Q, et al. Assessment of pulmonary physiological changes caused by aging, cigarette smoking, and COPD with hyperpolarized ^{129}Xe magnetic resonance. *Eur Radiol.* 2024;34:7450-7459. <https://doi.org/10.1007/s00330-024-10800-w>
71. Liu X, Li H, Li H, et al. Measurement of pulmonary hematocrit using oscillation of hyperpolarized Xe MR signals in blood. *Magn Reson Med.* 2025;93:1886-1895. <https://doi.org/10.1002/mrm.30398>
72. Li H, Zhang Z, Zhao X, et al. Quantitative evaluation of pulmonary gas-exchange function using hyperpolarized ^{129}Xe CEST MRS AND MRI. *NMR Biomed.* 2018;31:e3961. <https://doi.org/10.1002/nbm.3961>
73. Li H, Li H, Zhang M, Huang C, Zhou X. Direct imaging of pulmonary gas exchange with hyperpolarized xenon MRI. *Innovation.* 2024;5:100720. <https://doi.org/10.1016/j.xinn.2024.100720>
74. Niedbalski PJ, Castro M. Using the full power of multiple hyperpolarized ^{129}Xe contrasts to interrogate aging, smoking, and COPD. *Eur Radiol.* 2024. <https://doi.org/10.1007/s00330-024-10822-4>
75. Zhang M, Li H, Li H, et al. Quantitative evaluation of lung injury caused by $\text{PM}_{2.5}$ using hyperpolarized gas magnetic resonance. *Magn Reson Med.* 2020;84:569-578. <https://doi.org/10.1002/mrm.28145>
76. Zhang M, Li H, Li H, et al. Dynamic evaluation of acute lung injury using hyperpolarized ^{129}Xe magnetic resonance. *NMR Biomed.* 2024;37:e5078. <https://doi.org/10.1002/nbm.5078>
77. Zhang Z, Li H, Xiao S, et al. Hyperpolarized gas imaging in lung diseases: functional and artificial intelligence perspective. *Acad Radiol.* 2024;31:4203-4216. <https://doi.org/10.1016/j.acra.2024.01.014>
78. Duan C, Deng H, Xiao S, et al. Fast and accurate reconstruction of human lung gas MRI with deep learning. *Magn Reson Med.* 2019;82:2273-2285. <https://doi.org/10.1002/mrm.27889>
79. Duan C, Deng H, Xiao S, et al. Accelerate gas diffusion-weighted MRI for lung morphometry with deep learning. *Eur Radiol.* 2022;32:702-713. <https://doi.org/10.1007/s00330-021-08126-y>
80. Li Z, Xiao S, Wang C, et al. Encoding enhanced complex CNN for accurate and highly accelerated MRI. *IEEE Trans Med Imaging.* 2024;43:1828-1840. <https://doi.org/10.1109/tmi.2024.3351211>
81. Shi S, Wang C, Xiao S, et al. Magnetic resonance image denoising for Rician noise using a novel hybrid transformer-CNN network (HTC-net) and self-supervised pretraining. *Med Phys.* 2024. <https://doi.org/10.1002/mp.17562>
82. Li Z, Xiao S, Wang C, et al. Complementation-reinforced network for integrated reconstruction and segmentation of pulmonary gas MRI with high acceleration. *Med Phys.* 2024;51:378-393. <https://doi.org/10.1002/mp.16591>
83. Zhang J, Jiang W, Luo Q, et al. Rational design of hyperpolarized xenon NMR molecular sensor for the selective and sensitive determination of zinc ions. *Talanta.* 2014;122:101-5. <https://doi.org/10.1016/j.talanta.2014.01.023>
84. Guo Q, Zeng Q, Jiang W, et al. A molecular imaging approach to mercury sensing based on hyperpolarized Xe molecular clamp probe. *Chemistry (Easton).* 2016;22:3967-70. <https://doi.org/10.1002/chem.201600193>
85. Zhao L, Guo Q, Yuan C, et al. Photosensitive MRI biosensor for BCRP-targeted uptake and light-induced inhibition of tumor cells. *Talanta.* 2021;233:122501. <https://doi.org/10.1016/j.talanta.2021.122501>
86. Yuan C, Guo Q, Zeng Q, et al. Dual-signal chemical exchange saturation transfer (Dusi-CEST): an efficient strategy for visualizing drug delivery monitoring in living cells. *Anal Chem.* 2024;96:1436-1443. <https://doi.org/10.1021/acs.analchem.3c03408>
87. Yang Y, Zhang Y, Wang B, et al. Coloring ultrasensitive MRI with tunable metal-organic frameworks. *Chem Sci.* 2021;12:4300-4308. <https://doi.org/10.1039/d0sc06969h>
88. Zeng Q, Bie B, Guo Q, et al. Hyperpolarized Xe NMR signal advancement by metal-organic framework entrapment in aqueous solution. *Proc Natl Acad Sci U S A.* 2020;117:17558-17563. <https://doi.org/10.1073/pnas.2004121117>
89. Yue Q, Zeng Q, Guo Q, et al. Pitaya-inspired metal-organic framework nanozyme for multimodal imaging-guided synergistic cuproptosis, nanocatalytic therapy, and photothermal therapy. *Adv Healthc Mater.* 2024;13:e2402915. <https://doi.org/10.1002/adhm.202402915>
90. Zhang X, Yang Y, Yuan Y, et al. Hyperpolarized ^{129}Xe atoms sense the presence of drug molecules in nanohosts revealed by magnetic resonance imaging. *Anal Chem.* 2024;96:10152-10160. <https://doi.org/10.1021/acs.analchem.3c05573>
91. Yang S, Yuan Y, Jiang W, et al. Hyperpolarized ^{129}Xe magnetic resonance imaging sensor for H_2S . *Chemistry.* 2017;23:7648-7652. <https://doi.org/10.1002/chem.201605768>
92. Yang S, Jiang W, Ren L, et al. Biothiol xenon MRI sensor based on thiol-addition reaction. *Anal Chem.* 2016;88:5835-40. <https://doi.org/10.1021/acs.analchem.6b00403>
93. Zeng Q, Guo Q, Yuan Y, et al. Mitochondria targeted and intracellular biothiol triggered hyperpolarized ^{129}Xe magnetofluorescent biosensor. *Anal Chem.* 2017;89:2288-2295. <https://doi.org/10.1021/acs.analchem.6b03742>
94. Zeng Q, Guo Q, Yuan Y, et al. Ultrasensitive molecular building block for biothiol NMR detection at picomolar concentrations. *iScience.* 2021;24:103515. <https://doi.org/10.1016/j.isci.2021.03515>
95. Zeng Q, Guo Q, Yuan Y, et al. Protocol for detecting substrates in living cells by targeted molecular probes through hyperpolarized ^{129}Xe MRI. *STAR Protocols.* 2022;3:101499. <https://doi.org/10.1016/j.xpro.2022.101499>
96. Zhang B, Guo Q, Luo Q, et al. An intracellular diamine oxidase triggered hyperpolarized ^{129}Xe magnetic resonance biosensor. *Chem Commun (Camb).* 2018;54:13654-13657. <https://doi.org/10.1039/c8cc07822j>
97. Saunders LC, Collier GJ, Chan HF, et al. Longitudinal lung function assessment of patients hospitalized with COVID-19 using ^1H and ^{129}Xe lung MRI. *Chest.* 2023;164:700-716. <https://doi.org/10.1016/j.chest.2023.03.024>
98. Biederer J. MR imaging of the airways. *Br J Radiol.* 2023;96:20220630. <https://doi.org/10.1259/bjr.20220630>
99. The State Council's General Office of the People's Republic of China. State council measures to enhance people's fitness, health.2019. Accessed January 23, 2025. https://english.www.gov.cn/policies/latestreleases/201907/15/content_WS5d2c6f8fc6d05cbd94d67a02.html
100. Youth Group of Chinese Society of Radiology Chinese Medical Association, MRI Group of Chinese Society of Radiology Chinese Medical Association, Cardio-Thoracic Group of Chinese Society of Radiology Chinese Medical Association. Consensus on the clinical standardization of hyperpolarized ^{129}Xe pulmonary functional MR imaging techniques. *Chin J Radiol.* 2025;59:635-643. <https://doi.org/10.3760/cma.j.cn112149-20250303-00111>

© The Author(s) 2025. Published by Oxford University Press on behalf of the British Institute of Radiology. All rights reserved. For commercial re-use, please contact reprints@oup.com for reprints and translation rights for reprints. All other permissions can be obtained through our RightsLink service via the Permissions link on the article page on our site—for further information please contact journals.permissions@oup.com.

British Journal of Radiology, 2025, 00, 1–11

<https://doi.org/10.1093/bjr/tqaf119>

Review